Shah et al. *Boundary Value Problems* (2017) 2017:94
DOI 10.1186/s13661-017-0827-4

Boundary Value Problems
a SpringerOpen Journal

RESEARCH Open Access

MHD Carreau fluid slip flow over a porous stretching sheet with viscous dissipation and variable thermal conductivity

Rehan Ali Shah[1*], Tariq Abbas[2], Muhammad Idrees[2] and Murad Ullah[2]

*Correspondence:
mmrehan79@yahoo.com
[1]Department of Basic Sciences and Islamiat, University of Engineering and Technology Peshawar, Khyber Pakhtoon Khwa, Pakistan
Full list of author information is available at the end of the article

Abstract

The aim of this article is to investigate MHD Carreau fluid slip flow with viscous dissipation and heat transfer by taking the effect of thermal radiation over a stretching sheet embedded in a porous medium with variable thickness and variable thermal conductivity. Thermal conductivity of the fluid is assumed to vary linearly with temperature. The constitutive equations of Carreau fluid are modeled in the form of partial differential equations (PDEs). Concerning boundary conditions available, the PDEs are converted to ordinary differential equations (ODEs) by means of similarity transformation. The homotopy analysis method (HAM) is used for solution of the system of nonlinear problems. The effects of various parameters such as Weissenberg number We^2, magnetic parameter M^2, power law index n, porosity parameter D, wall thickness parameter α, power index parameter m, slip parameter λ, thermal conductivity parameter ε, radiation parameter R and Prandtl number on velocity and temperature profiles are analyzed and studied graphically.

Keywords: magnetohydrodynamics (MHD); Carreau fluid flow; stretching sheet; slip flow; variable thickness; variable thermal conductivity; thermal radiation

1 Introduction

The study of heat transfer and boundary layer flow over a stretching sheet has received a great deal of attention from many researchers due to its importance in many engineering and industrial applications, such as paper production, glass-fiber production, solidification of liquid crystals, petroleum production, exotic lubricants, suspension solutions, wire drawing, continuous cooling and fibers spinning, manufacturing plastic films and extraction of polymer sheet. Crane [1] was the first person who studied the boundary layer flow past a stretching sheet. He concluded that velocity is proportional to the distance from the slit. Gupta and Gupta [2] discussed the problem of the continuous moving surface with constant temperature. The constant surface velocity case with a power law temperature variation was studied by Soundalgekar et al. [3]. Elbashbeshy [4] examined the heat transfer over a stretching surface with variable heat flux and uniform surface heat flux. Grubka et al. [5] studied the stretching flow problem with a variable surface temperature. Hayat et al. [6] obtained the series solutions for stretching sheet problem with mixed convection by using the homotopy analysis method (HAM). In the presence of a transverse magnetic field, Chaim [7] studied boundary layer flow due to a plate stretching with a power law

velocity. Effect of variable thermal conductivity and heat source/sink on flow near a stagnation point on a nonconducting stretching sheet was studied by Sharma et al. [8].

Georgiou [9] investigated time-dependent Poiseuille flow of Carreau fluid in the presence of slip effect and concluded that the wavelength and amplitude of oscillations in radial direction decrease with an increase in the slip effect. The peristaltic flow characteristics of Carreau fluid in a uniform tube and the heat transfer characteristics of Carreau fluid were discussed by El Hakeem [10]. Malik et al. [11] studied the pressure-dependent viscosity in Carreau fluid through a porous medium. The effect of transpiration on magnetohydrodynamic stagnation-point flow of Carreau nanofluid toward a stretching/shrinking sheet in the presence of thermophoresis and Brownian motion was numerically investigated by Sulochana et al. [12]. Akbar et al. [13] investigated numerically the flow of peristaltic Carreau nanofluid past an asymmetric channel and found that increasing values of magnetic parameter encourage the velocity profiles. Ali and Hayat [14] presented the analytic solution of mathematical modeling for the flow of incompressible Carreau fluid in an asymmetric channel with sinusoidal wall variations. Suneetha et al. [15] investigated the effect of thermal radiation on a two-dimensional stagnation point flow of an incompressible MHD Carreau fluid towards a shrinking surface in the presence of convective boundary conditions. The unsteady peristaltic flow of an incompressible Carreau fluid in eccentric cylinders was investigated by Nadeem et al. [16]. The boundary layer flow and heat transfer to a Carreau model over a nonlinear stretching surface was discussed by Khan et al. [17]. Masood et al. [18] investigated the effect of magnetic field on the stagnation point flow of a generalized Newtonian Carreau fluid.

The problem of free convection about a vertical impermeable flat plate in a Darcy porous medium was studied by Cheng et al. [19]. The heat transfer and flow in a porous medium over a stretching surface with internal heat generation and suction or blowing when the surface is held at a constant temperature was studied by Elbashbeshy et al. [20]. Using the homotopy analysis method, analytic solution was obtained by Hayat et al. [21] for the flow through a porous medium. Fang et al. [22] studied the boundary layer over a continuously stretching sheet with variable thickness. The progress of thermal diffusive flow over a stretching sheet with variable thickness was investigated by Subhashini et al. [23]. Khader et al. [24] obtained the numerical solution for the flow and heat transfer in a thin liquid film over an unsteady stretching sheet in a saturated porous medium in the presence of thermal radiation by using the finite difference method. Mostafa et al. [25] studied the flow and heat transfer of an electrically conducting non-Newtonian power law fluid within a thin liquid film over an unsteady stretching sheet in the presence of a transverse magnetic field with variable viscosity and variable thermal conductivity. Anjali Devi et al. [26] studied the boundary layer and heat transfer characteristics of hydromagnetic flow over a stretching sheet with variable thickness. Numerical solution for the flow of a Newtonian fluid over an impermeable stretching sheet with a power law surface velocity, slip velocity and variable thickness was studied by Megahed et al. [27]. Eid et al. [28] studied numerical solutions for the slip flow and heat transfer of a Newtonian fluid due to an impermeable stretching sheet which is embedded in a porous medium with a power law surface velocity and variable thickness in the presence of thermal radiation, viscous dissipation and slip velocity effects. The heat and mass transfer in Carreau fluid flow over a permeable stretching sheet with convective slip conditions in the presence of applied magnetic field, nonlinear thermal radiation, cross diffusion and suction/injection effects was numerically studied

by Gnaneswara et al. [29]. Groza et al. [30] presented a Newton interpolating series for approximate solutions of the entire functions of multipoint boundary value problems for differential equations. Marin [31] extended the concept of domain of influence, proposed by Cowin and Nunziato, in order to cover the elasticity of micro stretch materials. Ghita et al. [32] formulated some problems modeling the local hardening behavior of a plastic material following a Prandtl-Reuss law. Directional linear hardening, which is similar to Bauschinger's effect in metals, is characterized by an anisotropic factor. The magnetohydrodynamic (MHD) flow of non-Newtonian nanofluid in a pipe was studied by Ellahi [33]. Ellahi et al. [34] theoretically investigated the problem of the peristaltic flow of Jeffrey fluid in a non-uniform rectangular duct under the effects of Hall and ion slip. Marin et al. [35] considered a right cylinder composed of a physically micropolar thermoelastic material for which one plane end is subjected to an excitation harmonic in time.

The aim of the present work is to model and analyze the steady boundary layer flow of MHD Carreau fluid slip flow with viscous dissipation and heat transfer by taking the effects of thermal radiation over a stretching sheet embedded in a porous medium with variable thickness and variable thermal conductivity. The system of nonlinear partial differential equations is transformed into a system of ordinary differential equations using appropriate similarity transformations. A model system of equations is solved analytically by means of the homotopy analysis method (HAM).

2 Mathematical formulation

2.1 Description of the problem

Consider two-dimensional steady boundary layer flow of MHD Carreau fluid slip flow over a stretching sheet embedded in a porous medium. The origin is located at the slit, through the sheet is drawn in the fluid medium. The x-axis is taken in the direction of sheet motion, and the y-axis is normal to it. The sheet is stretched with velocity $U_w = U_0(x+b)^m$, where U_0 is the reference velocity. Assume that the sheet is not flat, which is specified as $y = A(x+b)^{\frac{1-m}{2}}$, where the coefficient A is chosen small for the sheet to be sufficiently thin, and m is the velocity power index. The problem is valid for $m \neq 1$ because for $m = 1$, the problem reduces to a flat sheet.

2.2 Governing equations and boundary conditions

The basic governing equations of continuity, boundary layer flow and heat transfer are

$$\frac{\partial u}{\partial x} + \frac{\partial v}{\partial y} = 0, \tag{1}$$

$$u\frac{\partial u}{\partial x} + v\frac{\partial u}{\partial y} = \nu\frac{\partial^2 u}{\partial y^2} - \frac{\mu}{\rho k}u + 3\nu\frac{(n-1)}{2}\Gamma^2\left(\frac{\partial u}{\partial y}\right)^2\frac{\partial^2 u}{\partial y^2} - \frac{\sigma J^2}{\rho}u, \tag{2}$$

$$\rho c_p\left(u\frac{\partial T}{\partial x} + v\frac{\partial T}{\partial y}\right) = \frac{\partial}{\partial y}\left(\kappa\frac{\partial T}{\partial y}\right) - \frac{\partial q_r}{\partial y} + \mu\left(\frac{\partial u}{\partial y}\right)^2, \tag{3}$$

where the velocity components u and v are along the x and y axes, ν, ρ and σ are the kinematic viscosity, fluid density and electrical conductivity, respectively. Other parameters, such as the acceleration due to gravity is g, T is the fluid temperature, κ is the thermal diffusivity, Γ is the time constant, J is the magnetic field, k is the permeability of the porous medium, q_r is the radiative heat flux, c_p is the specific heat at constant pressure and n is the power law index. For $n = 1$, the Carreau model reduces to the Newtonian one.

The radiative heat flux q_r is employed according to Rosseland approximation [36] such that

$$q_r = \frac{4\sigma^*}{3k^*}\frac{\partial T^4}{\partial y}, \tag{4}$$

where $\sigma^* = 5.6696 \cdot 10^{-8}$ W m^{2}K^{-4} is the Stefan-Boltzmann constant and k^* is the mean absorption coefficient. Following Rapits [37], we assume that the temperature differences within flow are sufficiently small such that T^4 may be expressed as a linear function of the temperature. Expanding T^4 in a Taylor series about T_∞ and neglecting higher order terms, we have

$$T^4 \cong 4T_\infty^3 T - 3T_\infty^4. \tag{5}$$

The physical and mathematical advantage of the Rosseland formula (4) consists in the fact that it can be combined with Fourier's second law of conduction to an effective conduction-radiation flux q_{eff} in the form

$$q_{\text{eff}} = -\left(\kappa + \frac{16\sigma^* T_\infty^3}{3k^*}\right)\frac{\partial T}{\partial y} = -\kappa_{\text{eff}}\frac{\partial T}{\partial y}, \tag{6}$$

where $\kappa_{\text{eff}} = (\kappa + \frac{16\sigma^* T_\infty^3}{3k^*})$ is the effective thermal conductivity. So, the steady energy balance equation, including the net contribution of the radiation emitted from the hot wall and observed in the colder fluid, takes the form

$$\rho c_p\left(u\frac{\partial T}{\partial x} + v\frac{\partial T}{\partial y}\right) = \frac{\partial}{\partial y}\left(\kappa_{\text{eff}}\frac{\partial T}{\partial y}\right) + \mu\left(\frac{\partial u}{\partial y}\right)^2. \tag{7}$$

To obtain the similarity solutions, it is assumed that the permeability of the porous medium $k(x)$ is of the form $k(x) = k_0(x+b)^{1-m}$, where k_0 is the permeability parameter.

The corresponding equations are subjected to the boundary conditions

$$\begin{aligned} &u(x,y) = U_0(x+b)^m + \lambda_1\left(\frac{\partial u}{\partial y}\right), \qquad v(x,y) = 0, \\ &T(x,y) = T_w \quad \text{at } y = A(x+b)^{\frac{1-m}{2}}, \end{aligned} \tag{8}$$

$$u(x,y) = 0, \qquad T(x,y) = 0 \quad \text{at } y \to \infty, \tag{9}$$

where λ_1 is the slip coefficient having dimension of length. For similarity solutions, it is assumed that the slip coefficient λ_1 is of the form $\lambda_1 = (x+b)^{\frac{1-m}{2}}$.

The mathematical analysis of the problem is simplified by introducing the following dimensionless coordinates:

$$\begin{aligned} &\eta = y\sqrt{U_0\left(\frac{m+1}{2}\right)\frac{(x+b)^{m-1}}{\nu}}, \\ &\psi(x,y) = \sqrt{\nu U_0\left(\frac{2}{m+1}\right)(x+b)^{m+1}}F(\eta), \\ &\Theta(\eta) = \frac{T - T_\infty}{T_w - T_\infty}, \end{aligned} \tag{10}$$

where η is the similarity variable, ψ is the stream function defined as $u = \frac{\partial \psi}{\partial y}$ and $v = -\frac{\partial \psi}{\partial x}$ and $\Theta(\eta)$ is the dimensionless temperature.

In this study, the equation for the dimensionless thermal conductivity κ is generalized for temperature dependence as follows:

$$\kappa = \kappa_\infty(1 + \xi\Theta), \tag{11}$$

where κ_∞ is the ambient thermal conductivity and ξ is the thermal conductivity parameter.

Using these variables, the boundary layer governing equations (1)-(3) can be written in a non-dimensional form as follows:

$$F''' + FF'' - DF' + \frac{3}{4}(n-1)(m+1)We^2F'''F''^2 - M^2F' - \frac{2m}{m+1}F'^2 = 0, \tag{12}$$

$$\left(\frac{1+R}{Pr}\right)\left((1+\xi\Theta)\Theta'' + \xi\Theta'^2\right) + F\Theta' + EcF'^2 = 0, \tag{13}$$

where $We^2 = \frac{\Gamma^2 U_0^3 (x+b)^{3m-1}}{\nu}$ is the Weissenberg number, $D = \frac{2\nu}{k_0 U_0 (m+1)}$ is the porosity parameter, $M^2 = \frac{\sigma^2 J_0^2}{\rho U_0}$ is the magnetic parameter, $Pr = \frac{\mu c_p}{\kappa_\infty}$ is the Prandtl number, $Ec = \frac{U_w^2}{c_p(T_w - T_\infty)}$ is the Eckert number and $R = \frac{16\sigma^* T_\infty^3}{3k^*\kappa_\infty}$ is the radiation parameter.

Boundary conditions (8)-(9) will be transformed

$$F(\alpha) = \alpha\left(\frac{1-m}{1+m}\right)\left[1 + \lambda F''(\alpha)\right], \qquad F'(\alpha) = 1 + \lambda F''(\alpha), \qquad \Theta(\alpha) = 1, \tag{14}$$

$$F'(\infty) = 0, \qquad \Theta(\infty) = 0, \tag{15}$$

where $\lambda = \frac{\sqrt{U_0(m+1)}}{\sqrt{2\nu}}$ is the slip velocity parameter, $\alpha = A\sqrt{\frac{U_0(m+1)}{2\nu}}$ is the parameter related to the sheet thickness, and $\eta = \alpha = A\sqrt{\frac{U_0(m+1)}{2\nu}}$ indicates the plate surface. In order to facilitate the computation, we introduce the function $f(\zeta) = f(\eta - \alpha) = F(\eta)$ and $\theta(\zeta) = \theta(\eta - \alpha) = \Theta(\eta)$. The similarity equations (12)-(13) for $f(\zeta)$ and the associated boundary conditions (14)-(15) become, respectively,

$$f''' + ff'' - Df' + \frac{3}{4}(n-1)(m+1)We^2f'''f''^2 - M^2f' - \frac{2m}{m+1}f'^2 = 0, \tag{16}$$

$$\left(\frac{1+R}{Pr}\right)\left((1+\xi\theta)\theta'' + \xi\theta'^2\right) + f\theta' + Ecf''^2 = 0, \tag{17}$$

$$f(0) = \alpha\left(\frac{1-m}{1+m}\right)\left[1 + \lambda f''(0)\right], \qquad f'(0) = 1 + \lambda f''(0), \qquad \theta(0) = 1, \tag{18}$$

$$f'(\infty) = 0, \qquad \theta(\infty) = 0, \tag{19}$$

where the prime denotes differentiation with respect to ζ. Based on the variable transformation, the solution's domain will be fixed from 0 to ∞.

The physical quantity of interest in this study is the skin friction coefficient C_f and the local Nusselt number Nu_x, which are defined as

$$C_f = -2\sqrt{\frac{m+1}{2}}Re_x^{\frac{-1}{2}}f''(0), \qquad Nu = -\sqrt{\frac{m+1}{2}}Re_x^{\frac{1}{2}}\theta'(0), \tag{20}$$

where $R_e(x) = \frac{U_w X}{\nu}$ is the local Reynolds number and $X = x + b$.

3 Solution by the homotopy analysis method

In this section we apply the HAM to obtain approximate analytical solutions of the MHD Carreau fluid slip flow with viscous dissipation and heat transfer by taking the effect of thermal radiation over a stretching sheet embedded in a porous medium with variable thickness and variable thermal conductivity. We select initial guesses and the linear operator for equations (16) and (17) as

$$f_0(z) = \frac{-e^{-z}(1 - e^z + m - me^z - \alpha e^z + m\alpha e^z)}{(1+m)(1+\lambda)}, \qquad \theta_0(z) = e^{-z}, \tag{21}$$

$$L_f = \frac{\partial^3 f}{\partial z^3} + \frac{\partial^2 f}{\partial z^2}, \qquad L_\theta = \frac{\partial^2 \theta}{\partial z^2} + \frac{\partial \theta}{\partial z}, \tag{22}$$

the above auxiliary linear operators have the following properties:

$$\begin{aligned} &L_f\left(c_1 + c_2 z + c_3 e^{-z}\right) = 0, \\ &L_\theta\left(c_4 + c_5 e^{-z}\right) = 0, \end{aligned} \tag{23}$$

where c_i (i = 1-5) are arbitrary constants. The zeroth order deformation problems can be obtained as

$$(1-q)L_f\left[\widehat{f}(z;q) - f_0(z)\right] = qh_f N_f\left[\widehat{f}(z;q)\right], \tag{24}$$

$$(1-q)L_\theta\left[\widehat{\theta}(z;q) - \theta_0(z)\right] = qh_\theta N_\theta\left[\widehat{f}(z;q), \widehat{\theta}(z;q)\right], \tag{25}$$

$$\begin{aligned} N_f\left[\widehat{f}(z;q), \widehat{\theta}(z;q)\right] = {} & \frac{\partial^3 \widehat{f}(z;q)}{\partial z^3} + \widehat{f}(z;q)\frac{\partial^2 \widehat{f}(z;q)}{\partial z^2} - \frac{2m}{m+1}\left(\frac{\partial \widehat{f}(z;q)}{\partial z}\right)^2 \\ & + \frac{3(n-1)(m+1)}{4} We^2 \left(\frac{\partial \widehat{f}(z;q)}{\partial z}\right)^2 \frac{\partial^3 \widehat{f}(z;q)}{\partial z^3} \\ & - M^2\left(\frac{\partial \widehat{f}(z;q)}{\partial z}\right) - D\left(\frac{\partial \widehat{f}(z;q)}{\partial z}\right), \end{aligned} \tag{26}$$

$$\begin{aligned} N_\theta\left[\widehat{\theta}(z;q)\right] = {} & (1+R)\left(\left(1 + \xi\widehat{\theta}(z;q)\right)\frac{\partial^2 \widehat{\theta}(z;q)}{\partial z^2} + \xi\left(\frac{\partial \widehat{\theta}(z;q)}{\partial z}\right)^2\right) \\ & + Pr\widehat{f}(z;q)\frac{\partial \widehat{\theta}(z;q)}{\partial z} + PrEc\left(\frac{\partial^2 \widehat{f}(z;q)}{\partial z^2}\right)^2, \end{aligned} \tag{27}$$

where q is an embedding parameter, h_f and h_θ are the non-zero auxiliary parameters and N_f, N_θ are nonlinear operators.

For $q = 0$ and $q = 1$, we have

$$\begin{aligned} &\widehat{f}(z;0) = f_0(z), \qquad \widehat{f}(z;1) = f(z), \\ &\widehat{\theta}(z;0) = \theta_0(z), \qquad \widehat{\theta}(z;1) = \theta(z). \end{aligned} \tag{28}$$

As the embedding parameter q increases from 0 to 1, $\widehat{f}(z;q)$ and $\widehat{\theta}(z;q)$ vary from their initial guesses f_0 and θ_0 to the exact solutions $f(z)$ and $\theta(z)$, respectively.

Taylor's series expansion of these functions yields

$$\begin{aligned} f(z;q) &= f_0(z) + \sum_{k=1}^{\infty} f_k(z) q^k, \\ \theta(z;q) &= \theta_0(z) + \sum_{k=1}^{\infty} \theta_k(z) q^k, \end{aligned} \tag{29}$$

where

$$\begin{aligned} f_k &= \frac{1}{k!} \frac{\partial^k f(z;q)}{\partial z^k} \bigg|_{q=0}, \\ \theta_k &= \frac{1}{k!} \frac{\partial^k \theta(z;q)}{\partial z^k} \bigg|_{q=0}. \end{aligned} \tag{30}$$

Keep in mind that the above series depends on h_f and h_θ. On the assumption that the non-zero auxiliary parameters are chosen so that equations (28) converge at $q = 1$, we have

$$\begin{aligned} f(z) &= f_0(z) + \sum_{k=1}^{\infty} f_k(z), \\ \theta(z) &= \theta_0(z) + \sum_{k=1}^{\infty} \theta_k(z). \end{aligned} \tag{31}$$

Differentiating k-times the zeroth order deformation of Eqs. (24) and (25) one has the kth order deformation equations as

$$L_f\big[f_k(z) - \chi_k f_{k-1}(z)\big] = h_f R_{f,k}(z), \tag{32}$$

$$L_\theta\big[\theta_k(z) - \chi_k \theta_{k-1}(z)\big] = h_\theta R_{\theta,k}(z), \tag{33}$$

where the boundary conditions (18) and (19) take the form

$$\begin{aligned} &f_k(0) = f_k'(0) = f_k'(\infty) = 0, \\ &\theta_k'(0) = \theta_k(\infty) = 0, \end{aligned} \tag{34}$$

$$\begin{aligned} R_{f,k}(z) = {} & \frac{\partial^3 f_{k-1}(z)}{\partial z^3} + \sum_{j=0}^{k-1} f_{k-1-j}(z) \frac{\partial^2 f_j(z)}{\partial z^2} - \big(M^2 + D\big) \frac{\partial f_{k-1}(z)}{\partial z} \\ & - \frac{2m}{m+1} \sum_{j=0}^{k-1} \frac{\partial f_{k-1-j}(z)}{\partial z} \frac{\partial f_k(z)}{\partial z} \\ & + \frac{3(n-1)(m+1)}{4} We^2 \sum_{j=0}^{k-1} \left[\frac{\partial^2 f_{k-1-j}(z)}{\partial z^2} \frac{\partial^2 f_k(z)}{\partial z^2} \right] \frac{\partial^3 f_{k-1}(z)}{\partial z^3} + \chi_k, \end{aligned} \tag{35}$$

$$\begin{aligned} R_{\theta,k}(z) = {} & (1+R) \left(\big(1 + \xi \theta_k(z)\big) \frac{\partial^2 \theta_{k-1}(z)}{\partial z^2} + \xi \sum_{j=0}^{k-1} \frac{\partial \theta_{k-1-j}(z)}{\partial z} \frac{\partial \theta_k(z)}{\partial z} \right) \\ & + Pr \sum_{j=0}^{k-1} f_{k-1-j}(z) \frac{\partial \theta_k(z)}{\partial z} + PrEc \sum_{j=0}^{k-1} \left[\frac{\partial^2 f_{k-1-j}(z)}{\partial z^2} \frac{\partial^2 f_k(z)}{\partial z^2} \right], \end{aligned} \tag{36}$$

$$\chi_k = \begin{cases} 1, & k > 1, \\ 0, & k = 1. \end{cases} \tag{37}$$

Finally, the general solution may be written as follows:

$$\begin{aligned} f_k(z) &= f_k^* + c_1 + c_2 z + c_3 e^{-z}, \\ \theta_k(z) &= \theta_k^* + c_4 + c_5 e^{-z}, \end{aligned} \tag{38}$$

where f_k^* and θ_k^* are the special solutions.

4 Error analysis

Before starting analysis of the problem, we first analyze the accuracy of the HAM on this specific problem. For this purpose Figures 1-4 are drawn and Tables 1 and 2 are constructed. Error profiles of f for $\lambda = 0.2$ and 0.25 are plotted in Figures 1 and 3 versus the order of approximations. It is observed that error is continuously reducing by increasing the order of approximation, and satisfactory error is achieved at the 20th order. The error for temperature distribution is shown in Figures 2 and 4 for $\lambda = 0.2$ and 0.25, respectively. From here one can observe that accuracy up to 10^{-6} is achieved on the 20th order approximation. The optimal values of convergence control parameter as well as the minimum values of total averaged squared residual error for various order of approximations is shown in the table. Notice that the table is made to observe the error for velocity and temperature fields for different orders of approximations. One can notice that error in velocity component f and in temperature θ decreases as we increase the order of approximations.

Figure 1 Error profile of f, taking $\lambda = 0.2$, $n = 0.5$, $We = 0.03$, $M = 0.05$, $Pr = 0.7$, $m = 0.001$, $\alpha = 0.2$, $D = 0.5$, $R = 0.05$, $Ec = 0.02$ and $\xi = 0.01$.

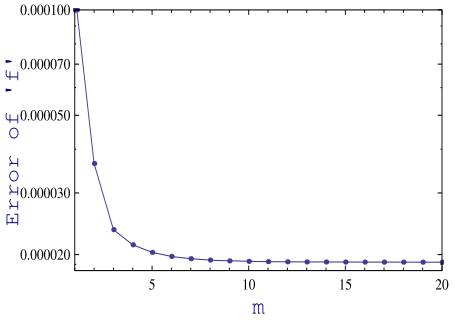

Figure 2 Error profile of θ, taking $\lambda = 0.2$, $n = 0.5$, $We = 0.03$, $M = 0.05$, $Pr = 0.7$, $m = 0.001$, $\alpha = 0.2$, $D = 0.5$, $R = 0.05$, $Ec = 0.02$ and $\xi = 0.01$.

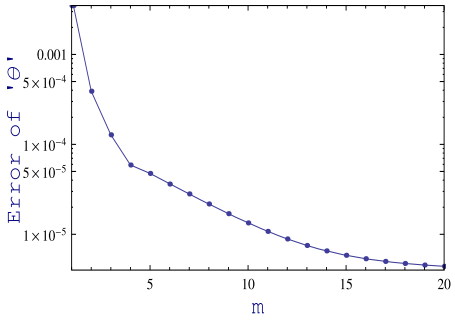

Figure 3 Error profile of f, taking $\lambda = 0.25$, $n = 0.5$, $We = 0.03$, $M = 0.05$, $Pr = 0.7$, $m = 0.001$, $\alpha = 0.2$, $D = 0.5$, $R = 0.05$, $Ec = 0.02$ and $\xi = 0.01$.

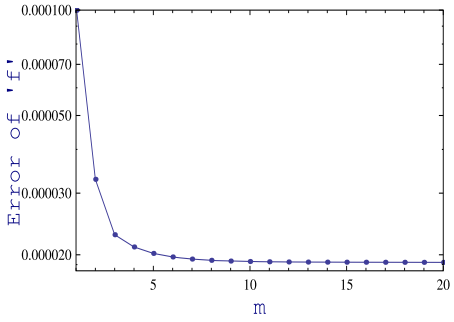

Figure 4 Error profile of θ, taking $\lambda = 0.25$, $n = 0.5$, $We = 0.03$, $M = 0.05$, $Pr = 0.7$, $m = 0.001$, $\alpha = 0.2$, $D = 0.5$, $R = 0.05$, $Ec = 0.02$ and $\xi = 0.01$.

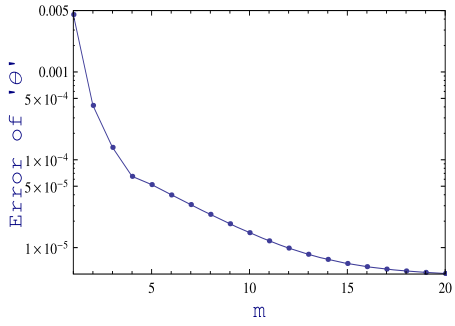

Table 1 Optimal value of convergence control parameters for different orders of approximations

Order of approximation	$\hbar_f$	$\hbar_\theta$	ε_m^t
2	−1.50039	−0.52479	7.16404×10^{-4}
3	−1.14981	−0.42060	6.90592×10^{-4}
4	−1.19560	−1.16693	5.15041×10^{-4}
5	−1.24825	−0.30060	5.55759×10^{-4}
6	−1.31412	−1.28875	5.01547×10^{-4}
7	−1.35632	−1.31419	4.05433×10^{-4}
8	−1.38483	−1.36406	2.18914×10^{-4}

Table 2 Individual averaged squared residual errors using optimal values of auxiliary parameters

m	ε_m^f	ε_m^θ
2	3.28588×10^{-5}	4.15975×10^{-4}
4	2.10586×10^{-5}	6.47816×10^{-5}
6	1.97175×10^{-5}	3.97772×10^{-5}
8	1.92867×10^{-5}	2.39297×10^{-5}
10	1.91356×10^{-5}	1.47931×10^{-5}
12	1.90796×10^{-5}	9.87921×10^{-6}
14	1.90562×10^{-5}	7.34606×10^{-6}
16	1.90439×10^{-5}	6.07003×10^{-6}
18	1.90350×10^{-5}	5.42235×10^{-6}
20	1.90271×10^{-5}	5.07083×10^{-6}

5 Results and discussion

In this article, the steady boundary layer flow of MHD Carreau fluid slip flow with viscous dissipation and heat transfer is studied by taking the effects of thermal radiation over a stretching sheet embedded in a porous medium with variable thickness and variable ther-

Figure 5 Velocity profile $f'(\eta)$ versus η for various values of D selecting fixed values for other parameters.

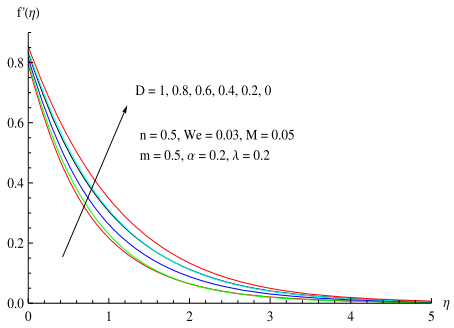

Figure 6 Temperature profile $\theta(\eta)$ versus η for various values of D selecting fixed values for other parameters.

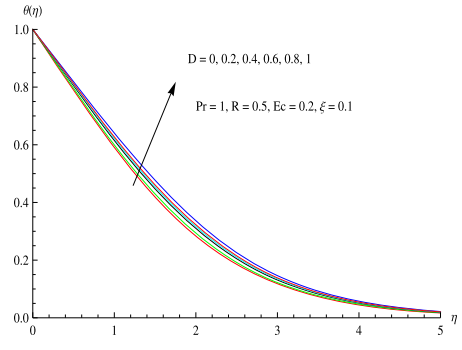

Figure 7 Velocity profile $f'(\eta)$ versus η for various values of α with $m = 5$ selecting fixed values for other parameters.

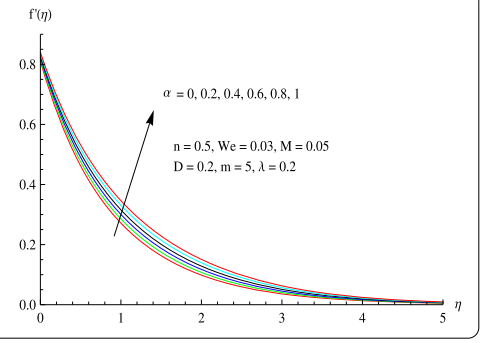

mal conductivity. The system of nonlinear ordinary differential equations (16)-(17) with boundary conditions (18) and (19) is solved analytically by HAM. The effects of Weissenberg number, power law index, magnetic parameter, velocity power index parameter, porous parameter, wall thickness parameter, slip velocity parameter, thermal conductivity parameter, radiation parameter, Eckert number and Prandtl number on the velocity and temperature fields are analyzed with the help of graphical aids and numerical results.

The effects of porosity parameter D on the velocity profile $f'(\eta)$ and temperature profile $\theta(\eta)$ are shown in Figures 5 and 6. It can be seen clearly that the velocity profile $f'(\eta)$ decreases as the magnitude of porosity parameter increases. Furthermore, boundary layer thickness decreases due to the increase in the porosity parameter, while the behavior of temperature profile decreases with an increase in the porosity parameter. The effects of wall thickness parameter α on the velocity profile $f'(\eta)$ have been analyzed and the results are presented in Figures 7 and 8. It is noticed that the velocity profile $f'(\eta)$ decreases at any point near to the plate as the wall thickness parameter increases for $m > 1$, the reverse

Figure 8 Velocity profile $f'(\eta)$ versus η for various values of α with $m = 0.5$ selecting fixed values for other parameters.

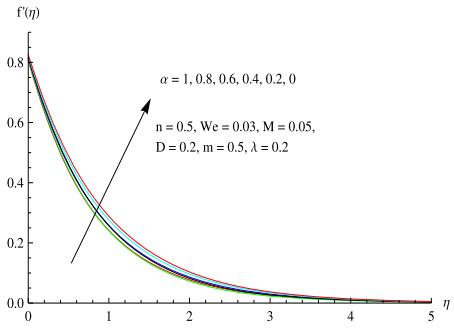

Figure 9 Velocity profile $f'(\eta)$ versus η for various values of λ selecting fixed values for other parameters.

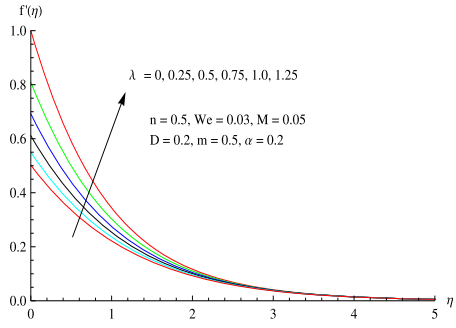

Figure 10 Temperature profile $\theta(\eta)$ versus η for various values of λ selecting fixed values for other parameters.

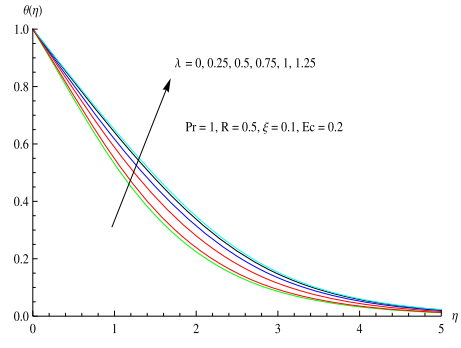

is true for $m < 1$. It is clear from figures that the thickness of the boundary layer becomes thicker for higher values of α when $m > 1$ and becomes thinner for higher values of α when $m < 1$.

The effect of the slip parameter λ on the velocity profile is shown in Figure 9. It is clear that the velocity profile decreases quickly throughout the fluid with the increase in the slip parameter λ. Boundary layer thickness decreases due to the effect of increasing the slip parameter λ while keeping other parameters fixed. The behavior of temperature distribution for the variation of the slip parameter λ is shown in Figure 10. It is obvious that the temperature profile increases with an increase in the slip parameter λ, while the other parameters are fixed.

The influence of velocity power index m on the velocity profile is displayed in Figure 11. The behavior of the velocity profile rises with a decrease in the values of velocity power index m. Thickness of boundary layer becomes thinner as m increases along the sheet

Figure 11 Velocity profile $f'(\eta)$ versus η for various values of m selecting fixed values for other parameters.

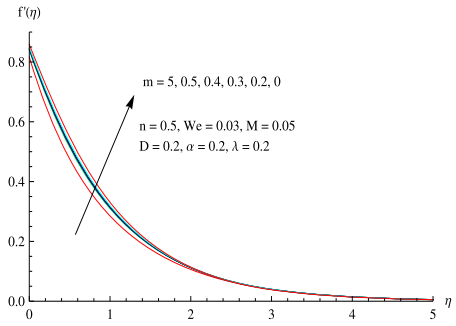

Figure 12 Velocity profile $f'(\eta)$ versus η for various values of M selecting fixed values for other parameters.

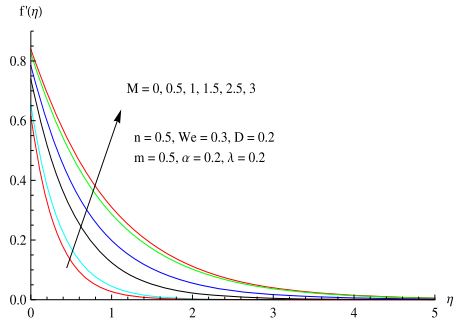

Figure 13 Temperature profile $\theta(\eta)$ versus η for various values of ξ selecting fixed values for other parameters.

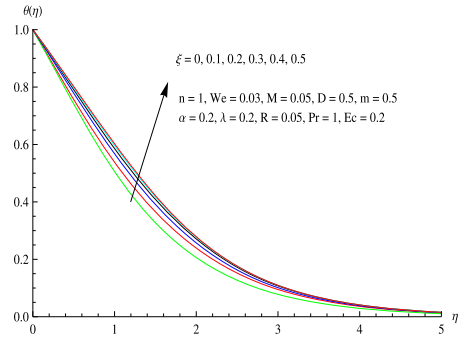

keeping the values of all other parameters fixed. Figure 12 depicts the velocity distribution for different values of M^2. As the magnetic parameter increases, the velocity distribution gets decreased. Further the boundary layer thickness is decreased due to the influence of magnetic parameter M^2 while keeping other parameters fixed.

The variation of thermal conductivity parameter on the temperature profile is shown in Figure 13. From here we see that the temperature profile as well as the thickness of thermal boundary layer increase when the thermal boundary parameter is increased. The effect of radiation parameter R on the temperature profile $\theta(\eta)$ is plotted in Figure 14. It is depicted that the temperature field and the thermal boundary layer thickness increase with the increase in R. Figure 15 displays the effect of Prandtl number on the temperature profile. It can be seen that the behavior of temperature distribution decreases with an increase in the Prandtl number. The temperature distribution for various values of Eckert number

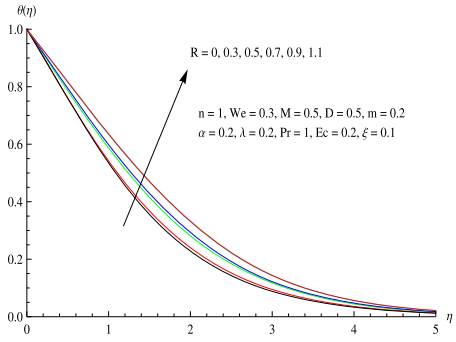

Figure 14 Temperature profile $\theta(\eta)$ versus η for various values of *R* selecting fixed values for other parameters.

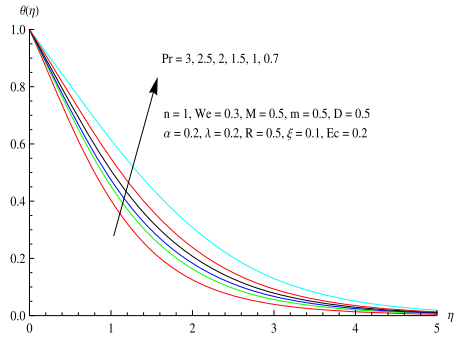

Figure 15 Temperature profile $\theta(\eta)$ versus η for various values of *Pr* selecting fixed values for other parameters.

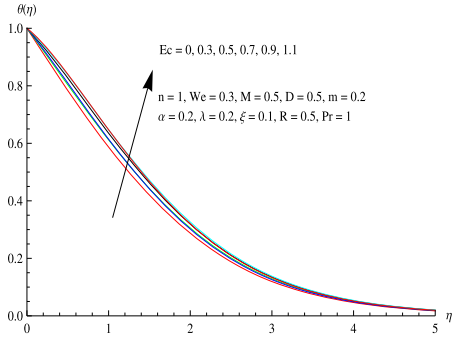

Figure 16 Temperature profile $\theta(\eta)$ versus η for various values of *Ec* selecting fixed values for other parameters.

Ec is plotted in Figure 16. It is that the temperature distribution $\theta(\eta)$ increases with the increase in the value of Eckert number *Ec* keeping the other parameters fixed.

In order to investigate the accuracy of (HAM), we compared the values of skin friction $-f''(0)$ with those given in Eid et al. [28] and Fang et al. [22] for the case $\alpha = 0.5$, $\alpha = 0.25$ when $We = 0$, $M = 0$, $\lambda = 0$, $n = 0.5$ and $D = 0$, respectively, for different values of velocity power index m.

The quantitative comparison is shown in Tables 3 and 4. Analytical and numerical results are found to be in good agreement. Table 5 demonstrates the effects of power law index, magnetic parameter, Weissenberg number, porosity parameter, wall thickness parameter, slip velocity parameter, velocity power index parameter, radiation parameter, Eckert number, thermal conductivity parameter and Prandtl number on the skin friction coefficient and the local Nusselt number. It is noticed that the skin friction coefficient increased but the local Nusselt number reduced with increasing porosity parameter and velocity

Table 3 Values of $-f''(0)$ for different values of m when $n = 0.5$, $We = 0$, $\lambda = 0$, $M = 0$, $D = 0$ and $\alpha = 0.5$

m	Present value	Eid et al. [28]	Fang et al. [22]
9.0	1.05992	1.0590	1.0589
7.0	1.05606	1.0551	1.0550
5.0	1.04963	1.0487	1.0486
3.0	1.03685	1.0359	1.0359
2.0	1.02422	1.0234	1.0234
1.0	1.00000	1.0000	1.0000
0.5	0.97665	0.9798	0.9799
0.0	0.95050	0.9575	0.9576
−1/3	0.99301	1.0000	1.0000
−0.50	1.15585	1.1668	1.1667

Table 4 Values of $-f''(0)$ for different values of m when $n = 0.5$, $We = 0$, $\lambda = 0$, $M = 0$, $D = 0$ and $\alpha = 0.25$

m	Present value	Eid et al. [28]	Fang et al. [22]
10.0	1.14419	1.1434	1.1433
9.0	1.14126	1.1404	1.1404
7.0	1.13314	1.1324	1.1323
5.0	1.11992	1.1185	1.1186
3.0	1.09168	1.0904	1.0905
1.0	1.00000	1.0000	1.0000
0.5	0.93225	0.9339	0.9338
0.0	0.77766	0.7842	0.7843
−1/3	0.46962	0.5000	0.5000
−0.50	0.13856	0.0834	0.0833

Table 5 Values of $-f''(0)$ and $-\theta'(0)$ for various values of m, D, α, λ, ξ, R, Ec, Pr

D	α	m	ξ	R	Pr	Ec	λ	n	We	M	$-f''(0)$	$-\theta'(0)$
0.0	0.2	0.5	0.1	0.5	1.0	0.2	0.2	0.5	0.3	0.5	0.825155	0.475184
0.5	-	-	-	-	-	-	-	-	-	-	0.974741	0.456129
1.0	-	-	-	-	-	-	-	-	-	-	1.099356	0.438155
0.5	0.0	0.5	0.1	0.5	1.0	0.2	0.2	0.5	0.3	0.5	0.957396	0.444435
-	0.25	-	-	-	-	-	-	-	-	-	0.979058	0.459059
-	0.0	1.0	-	-	-	-	-	-	-	-	1.008661	0.438441
-	0.25	-	-	-	-	-	-	-	-	-	1.005863	0.436451
0.5	0.2	0.0	0.1	0.5	1.0	0.2	0.2	0.5	0.3	0.5	0.914802	0.491316
-	-	0.5	-	-	-	-	-	-	-	-	0.974741	0.456129
-	-	1.0	-	-	-	-	-	-	-	-	1.006404	0.431844
0.5	0.2	0.5	0.0	0.5	1.0	0.2	0.2	0.5	0.3	0.5	0.974915	0.469772
-	-	-	0.2	-	-	-	-	-	-	-	0.974546	0.444876
-	-	-	0.5	-	-	-	-	-	-	-	0.972809	0.334618
0.5	0.2	0.5	0.1	0.5	1.0	0.2	0.2	0.5	0.3	0.5	0.974741	0.454128
-	-	-	-	0.7	-	-	-	-	-	-	0.974199	0.448591
-	-	-	-	1.0	-	-	-	-	-	-	0.973378	0.440501
0.5	0.2	0.5	0.1	0.5	0.7	0.2	0.2	0.5	0.3	0.5	0.974907	0.436983
-	-	-	-	-	1.0	-	-	-	-	-	0.974740	0.456128
-	-	-	-	-	3.0	-	-	-	-	-	0.977835	0.631131
0.5	0.2	0.5	0.1	0.5	1.0	0.0	0.2	0.5	0.3	0.5	0.974738	0.498102
-	-	-	-	-	-	0.5	-	-	-	-	0.974749	0.393482
-	-	-	-	-	-	1.0	-	-	-	-	0.974630	0.210871
0.5	0.2	0.5	0.1	0.5	1.0	0.2	0.0	0.5	0.3	0.5	1.300149	0.449268
-	-	-	-	-	-	-	0.5	-	-	-	0.724172	0.362024
-	-	-	-	-	-	-	1.0	-	-	-	0.514419	0.447731

Values of power law index, magnetic parameter and Weissenberg number are fixed.

power index parameter. Skin friction coefficient increases with an increase in the wall thickness parameter for $m = 0.5$ and 1. The local Nusselt number increases with an increase in the Prandtl number. Moreover, it is clear that the local Nusselt number decreases with an increase in the Eckert number, the thermal conductivity parameter and the radiation parameter. The effect of slip parameter is to decrease the skin friction coefficient.

6 Conclusion

In this article, similarity solution of the steady boundary layer flow of MHD Carreau fluid slip flow with viscous dissipation and heat transfer is analyzed by taking the effects of thermal radiation over a stretching sheet embedded in a porous medium with variable thickness and variable thermal conductivity. The characteristics of velocity and temperature profiles are studied graphically. The main conclusion can be summarized as follows:

- The increase in porosity parameter D, wall thickness parameter α, slip parameter λ and magnetic parameter M^2 leads to the decrease in velocity; on the other hand, velocity increases with an increase in velocity power index parameter.
- The increase in porous parameter D and Prandtl number Pr leads to the decrease in heat transfer.
- The increase in slip parameter λ, velocity power index parameter m, magnetic parameter M^2, thermal conductivity parameter ε radiation parameter R and Eckert number Ec leads to the increase in heat transfer.
- The increase in porosity parameter D, wall thickness parameter α and velocity power index parameter m leads to the increase in skin friction, while the skin friction coefficient decreases with an increase in slip parameter.
- The increase in Prandtl number Pr leads to the increase in local Nusselt number. The increase in porosity parameter D, velocity power index m, radiation parameter R, thermal conductivity parameter ε and Eckert number Ec leads to the decrease in local Nusselt number.

Acknowledgements
The authors would like to thank the reviewers for their constructive comments and valuable suggestions to improve the quality of the paper. This paper is self supported by authors in respect of funding and technically supported by Islamia Collogue University, KP, Peshawar, Pakistan.

Nomenclature
P: pressure ($N \cdot m^{-2}$); μ: viscosity ($m^2 \cdot s^{-1}$); ν: kinematic viscosity ($m^2 \cdot s^{-1}$); ρ: fluid density ($kg \cdot m^{-3}$); Γ: the time constant; u, v: x and y components of velocity ($m \cdot s^{-1}$); U_w: stretching surface velocity ($m \cdot s^{-1}$); x, y: spatial Cartesian coordinates (m); n: power law index; σ: electrical conductivity ($m^{-2} \cdot s$); c_p: specific heat (J/Kelvin); κ: thermal diffusivity ($W \cdot m^{-1} \cdot K^{-1}$); Pr: Prandtl number (ν/k); J: magnetic field ($k \cdot g^{1/2} \cdot m^{-1/2} \cdot s^{-1}$); S: suction parameter; T: fluid temperature (Kelvin); T_W: wall temperature (Kelvin); Nu_x: local Nusselt number; η: similarity variable; q_r: radiative heat flux (W/m^2); K: permeability of the porous medium; σ^*: Stefan-Boltzmann constant ($W \cdot m^{-2} \cdot K^{-4}$); k^*: mean absorption coefficient; k_0: permeability parameter; λ_1: slip coefficient; U_0: reference velocity ($m \cdot s^{-1}$); λ: slip velocity parameter; ξ: thermal conductivity parameter; Θ: dimensionless temperature; We^2: Weissenberg number; D: porosity parameter; Ec: Eckert number; R: radiation parameter; α: wall thickness parameter; T_∞: fluid ambient temperature (Kelvin); C_f: skin friction coefficient; $R_e(x)$: local Reynolds number; ψ: stream function.

Competing interests
The authors declare that they have no conflict of interests.

Authors' contributions
All authors participated in the analysis of the results and manuscript coordination. All authors read and approved the final manuscript.

Author details
[1]Department of Basic Sciences and Islamiat, University of Engineering and Technology Peshawar, Khyber Pakhtoon Khwa, Pakistan. [2]Department of Mathematics, Islamia College Peshawar, Khyber Pakhtoon Khwa, Pakistan.

Publisher's Note

Received: 4 January 2017 Accepted: 26 May 2017 Published online: 26 June 2017

References

1. Crane, LJ: Flow past a stretching Plate. Z. Angew. Math. Phys. **21**, 645-647 (1970)
2. Gupta, PS, Gupta, AS: Heat and mass transfer on a stretching sheet with suction or blowing. Can. J. Chem. Eng. **55**, 744-746 (1979)
3. Soundalgekar, VM, Ramana, TV: Heat past a continuous moving plate with variable temperature. Warme-und Stoffubertragung **14**, 91-93 (1980)
4. Elbashbeshy, EMA: Heat transfer over a stretching surface with variable surface heat flux. J. Phys. D, Appl. Phys. **31**, 1951-1954 (1998)
5. Grubka, LJ, Bobba, KM: Heat transfer characteristics of a continuous stretching surface with variable temperature. J. Heat Transf. **107**, 248-250 (1985)
6. Hayat, T, Abbas, Z, Javed, T: Mixed convection flow of a micropolar fluid over a non-linearly stretching sheet. Phys. Lett. A **372**, 637-647 (2008)
7. Chaim, TC: Hydromegnetic flow over a surface stretching with a power-law velocity. Int. J. Eng. Sci. **33**, 429-435 (1995)
8. Sharma, PR, Singh, G: Effects of variable thermal conductivity and heat source/sink on MHD flow near a stagnation point on a linearly stretching sheet. J. Appl. Fluid Mech. **2**, 13-21 (2009)
9. Georgiou, GC: The time-dependent, compressible Poiseuille and extrudate-swell flows of a Carreau fluid with slip at the wall. J. Non-Newton. Fluid Mech. **109**, 93-114 (2003)
10. El Hakeem, A, El Naby, A, El Misery, AEM: Separation in the flow through peristaltic motion of a Carreau fluid in uniform tube. Physica A **343**, 1-14 (2004)
11. Malik, MY, Zehra, I, Nadeem, S: Flows of carreau fluid with pressure dependent viscosity in a variable porous medium: application of polymer melt. Alex. Eng. J. **53**, 427-435 (2014)
12. Sulochana, C, Ashwinkumar, GP, Sandeep, N: Transpiration effect on stagnation-point flow of a Carreau nanofluid in the presence of thermophoresis and Brownian motion. Alex. Eng. J. **55**, 1-7 (2016)
13. Akbar, NS, Nadeem, S, Khan, ZH: Numerical simulation of peristaltic flow of a Carreau nanofluid in an asymmetric channel. Alex. Eng. J. **53**, 191-197 (2014)
14. Ali, N, Hayat, T: Peristaltic motion of a Carreau fluid in an asymmetric channel. Appl. Math. Comput. **193**, 535-552 (2007)
15. Suneetha, S, Gangadhar, K: Thermal radiation effect on MHD stagnation point flow of a Carreau fluid with convective boundary conditions. Appl. Math. Comput. **3**, 121-127 (2014)
16. Nadeem, S, Riaz, A, Akbar, NS, Elahi, R: Series solution of unsteady peristaltic flow of a Carreau fluid in eccentric cylinders. Ain Shams Eng. J. **5**, 293-304 (2013)
17. Khan, M, Hashim: Boundary layer flow and heat transfer to Carreau fluid over a nonlinear stretching sheet. AIP Advances **5**, 107203 (2015). doi:10.1063/1.4932627
18. Khan, M, Hashim, Alshomrani, AS: MHD stagnation-point flow of a Carreau fluid and heat transfer in the presence of convective boundary conditions. PLoS ONE **11**, e0157180 (2016)
19. Cheng, P, Minkowyez, WJ: Free convection about a vertical flat plate embedded in a porous medium with application to heat transfer from a dike. J. Geophys. Res. **82**, 2040-2044 (1977)
20. Elbashbeshy, EMA, Bazid, MAA: Heat transfer in a porous medium over a stretching surface with internal heat generation and suction or blowing. Appl. Math. Comput. **158**, 799-804 (2004)
21. Hayat, T, Abbas, Z, Pop, I, Asghar, S: Effects of radiation and magnetic field on the mixed convection stagnation point flow over a vertical stretching sheet in a porous medium. Int. J. Heat Mass Transf. **53**, 466-474 (2010)
22. Fang, T, Zhang, J, Zonng, Y: Boundary layer flow over a stretching sheet with variable thickness. Appl. Math. Comput. **218**, 7241-7252 (2012)
23. Subhashini, SV, Sumathi, R, Popb, I: Dual solutions in a thermal diffusive flow over a stretching sheet with variable thickness. Int. Commun. Heat Mass Transf. **48**, 61-66 (2013)
24. Khader, MM, Megahed, AM: Numerical simulation using the finite difference method for the flow and heat transfer in a thin liquid film over an unsteady stretching sheet in a saturated porous medium in the presence of thermal radiation. J. King Saud Univ., Eng. Sci. **25**, 29-34 (2013)
25. Mostafa, AAM, Megahed, AM: MHD flow and heat transfer in a non-Newtonian liquid film over an unsteady stretching sheet with variable fluid properties. Can. J. Phys. **87**, 1065-1071 (2009)
26. Anjali Devi, SP, Prakash, M: Steady nonlinear hydromagnetic flow over a stretching sheet with variable thickness and variable surface temperature. J. Korean Soc. Ind. Appl. Math. **18**, 245-256 (2014)
27. Khader, MM, Megahed, AM: Numerical solution for boundary layer flow due to a nonlinearly stretching sheet with variable thickness and slip velocity. Eur. Phys. J. Plus 100-128 (2013)
28. Eid, A, Khader, MM: Numerical studies using finite different method for viscous dissipation and thermal radiation effects on the slip flow and heat transfer due to a stretching sheet embedded in a porous medium with variable thickness and variable thermal conductivity. NTMSCI **4**, 38-50 (2016)
29. Gnaneswara, RM, Sandeep, N: Heat and mass transfer in radiative MHD Carreau fluid with cross diffusion. Ain Shams Eng. J. 1-16 (2016)
30. Groza, G, Khan, SM, Pop, N: Approximate solutions of boundary value problems for ODEs using Newton interpolating series. Carpath. J. Math. **25**(1), 73-81 (2009)
31. Marin, M: A domain of influence theorem for microstretch elastic materials. Nonlinear Anal., Real World Appl. **11**(5), 3446-3452 (2010)
32. Ghita, C, Pop, N, Cioban, H: Quasi-static behavior as a limit process of a dynamical one for an anisotropic hardening material. Comput. Mater. Sci. **52**(1), 217-225 (2012)
33. Ellahi, R: The effect of MHD and temperature dependent viscosity on the flow of non-Newtonian nanofluid in a pipe: analytic solutions. Appl. Math. Model. **37**, 1451-1457 (2013)

34. Ellahi, R, Bhatti, MM, Pop, I: Effect of Hall and Ion Slip on MHD Peristaltic of Jeffrey fluid in a nonuniform rectangular duct. Inter. J. for Num. Met. Heat and Fluid Flow **26** (2016)
35. Marin, M, Lupu, M: On harmonic vibrations in thermoelasticity of micropolar bodies. J. Vib. Control **4**, 507-518 (1998)
36. Rapits, A: Flow of a micropolar fluid past a continuously moving plate by the presence of radiation. Int. J. Heat Mass Transf. **41**, 2865-2866 (1998)
37. Rapits, A: Radiation and viscoelastic flow. Int. Commun. Heat Mass Transf. **26**, 889-895 (1999)